Original Research

In Vivo ^{31}P Magnetic Resonance Spectroscopic Imaging (MRSI) for Metabolic Profiling of Human Breast Cancer Xenografts

Morteza Esmaeili, MSc,[1]* Siver A. Moestue, PhD,[1,2] Bob C. Hamans, MSc,[3] Andor Veltien, BS,[3] Alexandr Kristian, MSc,[4,5] Olav Engebråten, PhD,[5,6] Gunhild M. Mælandsmo, PhD,[4] Ingrid S. Gribbestad, PhD,[1] Tone F. Bathen, PhD,[1] and Arend Heerschap, PhD[1,3]

Purpose: To study cancer associated with abnormal metabolism of phospholipids, of which several have been proposed as biomarkers for malignancy or to monitor response to anticancer therapy. We explored 3D ^{31}P magnetic resonance spectroscopic imaging (MRSI) at high magnetic field for in vivo assessment of individual phospholipids in two patient-derived breast cancer xenografts representing good and poor prognosis (luminal- and basal-like tumors).

Materials and Methods: Metabolic profiles from luminal-like and basal-like xenograft tumors were obtained in vivo using 3D ^{31}P MRSI at 11.7T and from tissue extracts in vitro at 14.1T. Gene expression analysis was performed in order to support metabolic differences between the two xenografts.

Results: In vivo ^{31}P MR spectra were obtained in which the prominent resonances from phospholipid metabolites were detected at a high signal-to-noise ratio (SNR >7.5). Metabolic profiles obtained in vivo were in agreement with those obtained in vitro and could be used to discriminate between the two xenograft models, based on the levels of phosphocholine, phosphoethanolamine, glycerophosphocholine, and glycerophosphoethanolamine. The differences in phospholipid metabolite concentration could partly be explained by gene expression profiles.

Conclusion: Noninvasive metabolic profiling by 3D ^{31}P MRSI can discriminate between subtypes of breast cancer based on different concentrations of choline- and ethanolamine-containing phospholipids.

Key Words: phospholipid; choline metabolism; phosphorus MR spectroscopic imaging; high field; ethanolamine kinase; basal-like
J. Magn. Reson. Imaging 2014;00:000–000.

ADVANCES IN MOLECULAR TECHNOLOGIES have contributed to a substantial increase of our knowledge of tumor growth. However, translating this knowledge to clinical practice is challenging. A noninvasive, reliable, and sensitive tool for the detection of biomarkers, such as certain metabolites relevant in the disease process, could improve this translation (1,2). In oncology, choline- and ethanolamine-containing phospholipids have attracted attention as potential metabolic biomarkers (3). They are major precursor molecules of cell membranes and play both structural and regulatory roles in cell metabolism and oncogenic signaling (3). To facilitate their use as biomarkers, a deeper understanding of their biology as well as noninvasive methods for their detection is needed.

Changes in the tissue levels of these metabolites can be recorded in vivo by magnetic resonance spectroscopy (MRS) (3). Proton (^{1}H) MRS has been widely used to study the increased total choline levels (tCho) in brain

[1]Department of Circulation and Medical Imaging, Norwegian University of Science and Technology (NTNU), Trondheim, Norway.
[2]St. Olavs University Hospital, P.O. Box 3250 Sluppen, N-7006, Trondheim, Norway.
[3]Department of Radiology, Radboud University Nijmegen Medical Center, Nijmegen, The Netherlands.
[4]Department of Tumor Biology, Institute for Cancer Research, Oslo University Hospital, Montebello, Oslo, Norway.
[5]Institute for Clinical Medicine, Faculty of Medicine, University of Oslo, Oslo, Norway.
[6]Department of Oncology, Oslo University Hospital, Oslo, Norway.
Contract grant sponsor: Norwegian University of Science and Technology (NTNU); Contract grant sponsor: Norwegian Cancer Society and the Norwegian Breast Cancer Society; Contract grant number: 2209215-2011; Contract grant sponsor: Norwegian Research Council; Contract grant number: 175459/V50, 186479/V50, 183379/S10, and 183621/S10; Contract grant sponsor: Liaison Committee between the Central Norway Regional Health Authority (RHA) and the Norwegian University of Science and Technology; Contract grant number: 46056655; Contract grant sponsor: Norwegian Research School in Medical Imaging (Travel grants M.E. and S.A.M.).
Present affiliation for Bob C. Hamans: Jeroen Bosch Hospital, Den Bosch, the Netherlands (BCH).
*Address reprint requests to: M.E., Department of Circulation and Medical Imaging, Norwegian University of Science and Technology (NTNU), P.O. Box 8905, N-7491 Trondheim, Norway. E-mail: m.esmaeili@ntnu.no
Received October 1, 2013; Accepted January 20, 2014.
DOI 10.1002/jmri.24588
View this article online at wileyonlinelibrary.com.

(4,5), prostate (6,7), and breast tumors (8). A response to therapy is often associated with a reduction in the tCho signal (9). However, in these spectra tCho is a combined signal, comprising several chemically distinct components; in particular, choline, phosphocholine (PCho), and glycerophosphocholine (GPC), which cannot be separated spectrally. This inability to separate contributions from PCho and GPC limits the diagnostic utility of in vivo ^{1}H MRS. The individual evaluation of each of these compounds might greatly aid differential tumor diagnosis and help to monitor the response of targeted anticancer therapies (10).

^{31}Phosphorus (^{31}P) MRS can detect phospholipid signals such as of GPC and PC and also of phosphoethanolamine (PEtn) and glycerophosphoethanolamine (GPE). In vivo ^{31}P MRS studies showed that malignant transformation is associated with elevated phosphomonoester (PME) levels (dominated by PCho and PEtn signals) and phosphodiesters (PDE) levels (dominated by GPC and GPE) (11). At higher magnetic field strength, the chemical shift differences between these signals increases, which enables the detection of individual PME and PDE compounds with in vivo ^{31}P MRS (12). To select ^{31}P MR spectra of tumor xenografts it is common to localize either only by the detection volume of a (surface) coil or by single voxel selection with an ISIS sequence or by 1D MR spectroscopic imaging (MRSI) (12–14).

The main objective of the present study was to investigate phospholipid metabolism of breast cancer xenografts in vivo by 3D ^{31}P MRSI at 11.7T. For this study we focused on a comparison of patient-derived luminal-like and basal-like breast cancer xenografts, as previous ex vivo studies have indicated that these two subtypes of breast cancer have distinct metabolic profiles (15,16).

MATERIALS AND METHODS

Animal Models

The two orthotopic xenograft models used involved direct implantation of primary human breast carcinoma tissue in severe combined immunodeficient BalbC nu/nu mice (17). The models, termed MAS98.12 and MAS98.06, grow in the mammary fat pad and represent basal-like (poor prognosis) and luminal-like (good prognosis) subtypes of human breast cancer, respectively. The animals were kept under pathogen-free conditions and received food and drinking water supplemented with 17-β-estradiol (4 μg/mL) to promote growth of the hormone-receptor-positive MAS98.06 xenografts.

All procedures and experiments involving animals were approved by The National Animal Research Authority, and carried out according to the European Convention for the Protection of Vertebrates used for Scientific Purposes.

In Vivo Measurement Protocol

For the in vivo MR experiments, 6 luminal-like and 10 basal-like xenografts were included. During MR scanning, the animals were anesthetized with 1.5% isoflurane and a mixture of O_2 and N_2O inhalation through a nasal mask. The animals were placed in a tube containing a tumor-sized cavity keeping the tumors immobilized. The tube cavity was positioned and fixed on the top and center of the solenoid surface coil assuring a reproducible positioning inside the magnet. Bed temperature was maintained at 37.5°C by applying warm air circulation. The respiration rate (~60 breaths/min) and body temperature were monitored by a rectal fiber optic temperature probe (Small Animal Instrument, NY).

In vivo ^{31}P 3D MRSI measurements were performed on a preclinical horizontal bore 11.7T MR system (Bruker BioSpec, Ettlingen, Germany). The spectra were recorded using homebuilt coils with a diameter of 16 mm (MRS of luminal-like xenografts) and of 12 mm (MRS of basal-like xenografts) tuned to 202.5 MHz for phosphorus. Localized ^{31}P MRSI spectra were obtained using a pulse acquire sequence with an adiabatic BIR-4 excitation pulse (18) with a flip angle of 45° over a spectral width of 40 ppm, Hanning-weighted Cartesian *k*-space sampling, repetition time (TR) of 2.5 seconds, matrix size of 8 × 8 × 8 interpolated to 16 × 16 × 16, field of view (FOV) of 50 × 50 × 50 $(mm)^3$, 3000 scans, 8 averages, and actual voxel size of about 1.1 cc (total scan time of 2 hr 5 min). Basic localization images were acquired prior to the MRSI to position the xenograft in the isocenter, subsequently followed by acquisition of coronal spin echo T_2-weighted images as an MRSI reference with the following parameters; TR/TE 1500/25 msec, FOV 50 × 50 mm^2, slice thickness 1 mm, and 9 consecutive slices covering the intense part of the tumor giving an acquisition time of 6 minutes 24 seconds. First- and second-order shimming was performed using FASTMAP (19). Selected ^{31}P MR spectra were analyzed from voxels of interest identified based on the coronal images of tumor tissue. The inhomogeneity of the magnetic field in breast tissues can be exacerbated by subject breathing, leading to poor shimming and ghosting artifacts (20). To overcome this, the MR experiments were performed using a simple but effective bed setup to immobilize the breast tumors, fixing the animal in prone position with the tumor protruding the bed into the surface coil.

In vivo ^{31}P MR spectra were processed using the java-based jMRUI software (21) and signals were fitted using the AMARES method (22). The postacquisition spectral processing included zero-filling of the FIDs into 4096 data points and 20 Hz exponential line broadening. Metabolites were quantified by normalizing the area under the peak to the total area under the detectable phospholipid signals within each voxel. An average SNR of 12.5 and 7.5 were measured ($SNR = S_{p\text{-}p}/N_{p\text{-}p}$; peak-to-peak signal intensity over the noise of the baseline) from MR spectra of basal-like and luminal-like xenografts, respectively.

Tumor volume was calculated using calipers to measure orthogonal sizes a and b and volume was estimated with ellipsoid formula; $vol = \pi(ab^2)/6$. MRS experiments were performed on the tumors with volume of 610.92 ± 139.02 mm^3 (mean ± SD) for

luminal-like and 885.98 ± 261.57 mm^3 for basal-like xenografts.

In Vitro ^{31}P NMR Experiments

For the in vitro NMR experiments, tissue samples (~45 mg) from the same animal models (but not the same animals as used for in vivo MRSI) were harvested ($n = 6$ from each model) and immediately frozen and stored in liquid nitrogen (−196°C) until extraction. The aqueous metabolites were extracted from the tissue samples with cold 7% perchloric acid (PCA) as described previously (23). The tumor tissues were pulverized and homogenized in PCA (1 mL per 50 mg tissue), using an ultrasound probe and centrifugation at 4400 rpm (5 min, at 4°C). The supernatant was neutralized with 1.0 M potassium hydroxide (KOH) and centrifuged once more. The new supernatant was transferred to cryotubes and stored at −80°C. Prior to NMR analysis, lyophilized supernatants were diluted (600 μL deuterium oxide [D_2O]) and transferred to NMR tubes (5 mm) after final neutralization with 1.0 M KOH (mean pH of 7.08).

NMR experiments were performed on a 14.1T Bruker spectrometer (Bruker Avance III 600 MHz/54 mm US-Plus) equipped with a multinuclear QCI CryoProbe (Bruker BioSpin). One-dimensional ^{1}H NMR spectra were recorded using a pulse-acquire sequence with presaturation pulses during relaxation delay and mixing time and two gradient pulses for efficient water suppression (Bruker; noesygppr1d), a 90° excitation pulse, a TR of 10.73 seconds, a sweep width of 20 ppm, and 32 free induction decays (FIDs) giving a total experiment time of 5 minutes. Single-pulse ^{31}P NMR spectra were recorded with a 30° excitation pulse, TR = 4 seconds, 12,096 FIDs, and a spectral region of 60 ppm. The in vitro ^{1}H/^{31}P NMR spectra were processed using the Bruker TopSpin v. 3.0 platform (Bruker BioSpin). Prior to Fourier transform, the accumulated FIDs were multiplied by an exponential function with a line-broadening factor of 3 Hz for ^{31}P (0.3 Hz for ^{1}H MR spectra). Phase and polynomial baseline corrections were performed on all spectra. Chemical shift was referenced to the GPC signal at 3.04 ppm (the Cr signal at 3.03 ppm for ^{1}H MR spectra). Spectral fitting was performed using the PeakFit software (PeakFit v. 4.12, SeaSolve Software, San Jose, CA). A mixed Gaussian-Lorenzian lineshape curve fitting function (24) was used after baseline correction. The fit correlation factor (r^2) obtained was better than 0.99 for all spectra. Metabolites were quantified by normalizing the area under the peak to the total area under the detectable phosphorylated signals of individual spectrum.

Gene Expression Analysis

Gene expression analysis was performed using previously generated microarray data (16). The differential expression of genes coding for enzymes directly involved in synthesis or degradation of PCho, PEtn, GPC, or GPE, as indicated by the KEGG glycerophospholipid pathway hsa:00564 (25), was analyzed using the same algorithm as in the previous study (16).

Statistical Analyses

The difference between in vivo and in vitro spectra of xenografts was evaluated by comparing the relative metabolite concentrations using an unpaired Mann–Whitney test (Prism GraphPad v. 4.03 Software, La Jolla, CA). The differences were considered statistically significant for P-values < 0.05. A t-test with empirical Bayesian correction of the test statistics were used for evaluating differential gene expression between the xenografts. To account for multiple testing, an adjusted P-value of 0.05 (using Benjamini & Hochberg's false discovery rate) was defined as the threshold for significant differential gene expression. Principal component analysis (PCA) was used to identify the major variation of all relative metabolite concentrations to evaluate the similarity of in vivo and in vitro spectra using MatLab 7.10.0.499 (MathWorks, Natick, MA).

RESULTS

In Vivo 3D ^{31}P MRSI Experiments

The xenograft tumors were identified in the T_2-weighted MR images (Fig. 1A, red arrows). A spectral map of the tumor area (of a basal-like xenograft) shows well-resolved ^{31}P MR spectra (Fig. 1B). Resonances of adenosine triphosphate (ATP), phosphocreatine (PCr), GPC, and GPE, inorganic phosphate (Pi), PCho, and PEtn were separately detected in ^{31}P MR spectra of basal-like (Fig. 1C) and luminal-like (Fig. 1D) xenografts. The ^{31}P-spectral profiles of the luminal-like and basal-like xenografts showed distinct differences, in particular in the spectral range between 2 and 8 ppm (Fig. 1C,D). With the same acquisition parameters, a slightly better SNR was achieved for the basal-like ^{31}P MR spectra compared to the luminal-like, most likely due to the use of a smaller coil and larger volume of the tumor.

The results from the relative quantification of phospholipid metabolites are given in Figure 2. The relative signals of PEtn and PCho levels were significantly higher in the luminal-like compared with the basal-like xenografts ($P < 0.001$ and $P < 0.05$, respectively). GPC and GPE were barely detectable in ^{31}P MR spectra of luminal-like xenografts and could only be quantified in three out of five MR spectra. GPC ($P < 0.001$) and GPE ($P < 0.01$) were significantly higher in the basal-like compared with the luminal-like xenografts. The PCho/GPC ($P < 0.01$) and PEtn/GPE ($P < 0.01$) ratios were significantly higher in the luminal-like xenografts compared with the basal-like xenografts.

In Vitro ^{31}P NMR Experiments

The in vitro ^{31}P NMR spectra obtained from luminal- and basal-like xenografts gave totally resolved

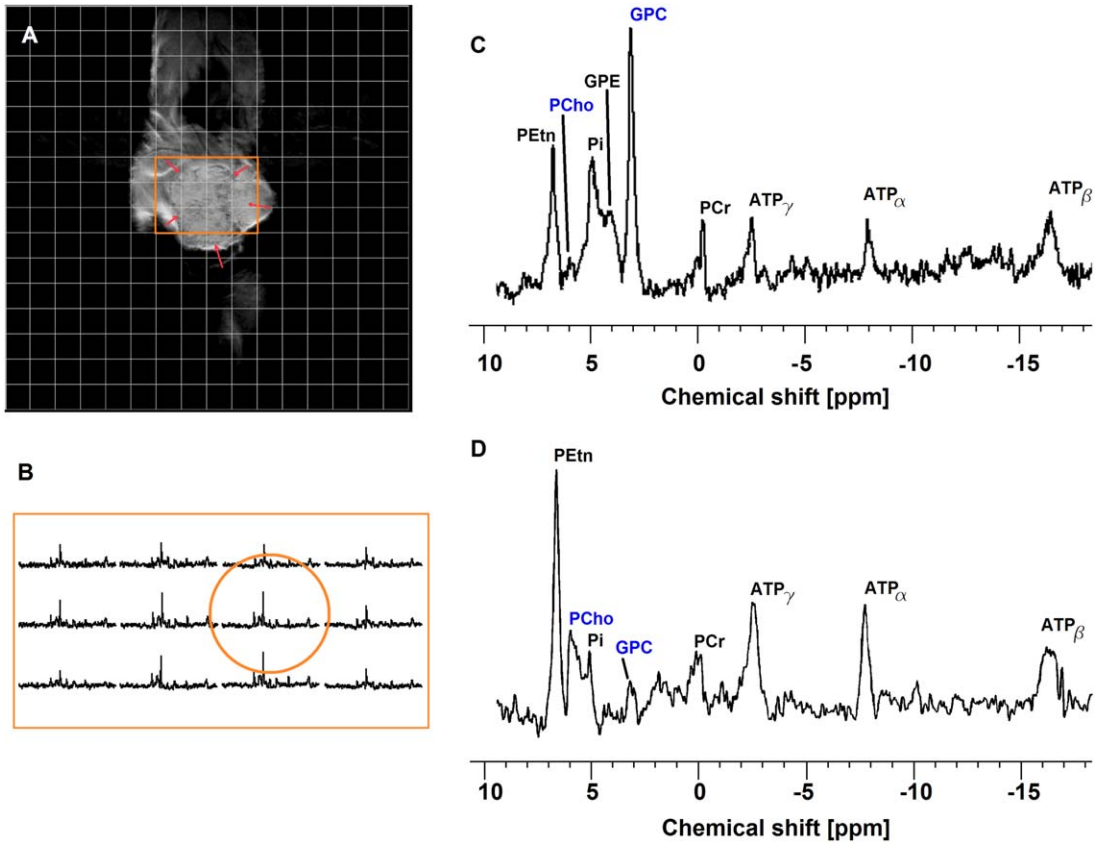

Figure 1. Choline- and ethanolamine-containing phospholipid metabolites in basal- and luminal-like xenografts. **A:** An interpolated ^{31}P MRSI grid (grid size of 8 × 8 × 8 interpolated to 16 × 16 × 16) overlaid on T_2-weighted MR image of a basal-like breast cancer xenograft (sagittal view). **B:** The voxels of interest were selected from the most central region of tumor tissues identified by T_2-weighted image (orange circle). MR spectra are presented from the box indicated in A (40 ppm spectral range). **C:** ^{31}P MR spectra from a basal-like (enlarged from B indicated by the orange circle) and (**D**) a luminal-like xenograft showing inverse relationship between PCho and GPC concentrations. High PCho and PEtn resonances were observed in the luminal-like xenografts, while GPC and GPE resonances were increased in the basal-like xenografts (the MR spectra in this figure are identically scaled). The assigned metabolite resonances are: PEtn, phosphoethanolamine; PCho, phosphocholine; Pi, inorganic phosphate; GPE, glycerophosphoethanolamine; GPC, glycerophosphocholine; PCr, phosphocreatine; ATP, adenosine triphosphate.

resonances for phospholipid metabolites (Fig. 3A,B). Pi was also observed in the ^{31}P NMR spectra of extracts but resonances from the high-energy phosphate metabolites PCr and ATP were not detected. Consistent with the in vivo data, the in vitro data analysis showed higher PEtn and PCho and lower GPC and GPE levels ($P < 0.001$ for all metabolites) in the luminal-like compared with the basal-like xenografts (Fig. 3). PCho/GPC and PEtn/GPE ratios were significantly higher in the luminal-like compared with the basal-like xenografts ($P < 0.01$ for both ratios). The PCho and GPC relationship observed in ^{31}P NMR spectra corresponded well with that observed in ^{1}H NMR spectra (Fig. 3C,D).

Comparison of In Vivo and In Vitro Measurements

The relative metabolite levels measured in in vitro and in vivo ^{31}P MR spectra were compared to validate how good in vivo ^{31}P MRSI is able to represent the same phospholipid profile as in vitro NMR. The two methods provided similar metabolic profiles (Figs. 1–3). No significant difference in metabolite levels between in vitro and in vivo spectra was found in the basal-like xenografts. Significant differences in PEtn ($P = 0.02$) and GPC ($P = 0.009$) levels were detected in the luminal-like xenografts (Fig. 3) between in vitro and in vivo MR spectra. However, the score plot from the PCA clearly shows that the differences in the metabolic profile obtained in vitro and in vivo within the luminal- or basal-like xenografts is much less than the difference between the two xenograft models (Fig. 4).

Gene Expression

Table 1 shows that the expression of 14 genes directly involved in the conversion of choline and ethanolamine to PCho and PEtn and degradation of phosphatidylcholine (PtdCho) and phosphatidylethanolamine (PtdEtn) to GPC and GPE were differentially expressed between the xenograft models. Higher expression of the genes *ethanolamine kinase 1* (*ETNK1*) and *2* (*ETNK2*) (involved in conversion of ethanolamine to PEtn) were found in the luminal xenografts compared with basal-like xenografts ($P < 0.001$), which are associated with a high PEtn level. Both *choline kinase* isoforms (*ChoKA* and *ChoKB* (involved in conversion from ethanolamine to PEtn and choline to PCho) were

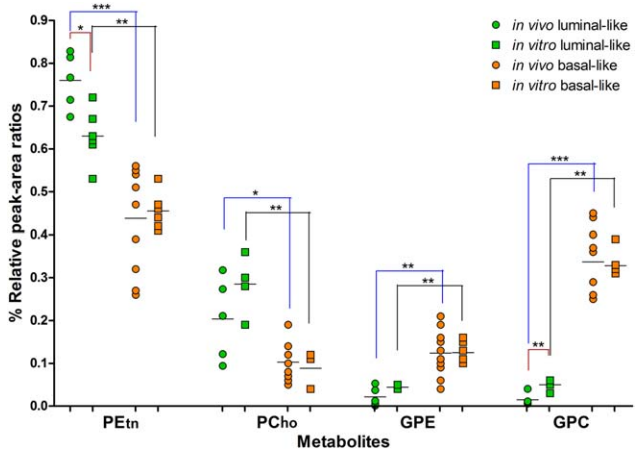

Figure 2. ^{31}P MRS results of phospholipid metabolites in breast cancer xenografts. Individual data points in the scatter-plot show the relative quantification of metabolites normalized to the sum of the four visible phospholipid metabolites within the voxels from in vivo and in vitro NMR data. Individual high-resolution ^{31}P NMR spectra of the tumor tissue extracts support the in vivo results. Comparing the MR spectra acquired in vivo with those in vitro, there was no significant difference in metabolite levels of the basal-like xenografts. The same analysis showed a significant difference between PEtn ($P = 0.02$) and GPC ($P = 0.009$) levels in the luminal-like xenografts. [Color figure can be viewed in the online issue, which is available at wileyonlinelibrary.com.]

also significantly higher expressed ($P < 0.001$) in the luminal-like xenografts. The high expression of these genes is in accordance with the higher concentration of PCho and PEtn in the luminal-like xenografts. The difference in GPC and GPE concentrations could not be directly elucidated from the gene expression data, as the differential expression of various phospholipases was complex and difficult to interpret. However, the *phospholipase A2 group IVA* (*PLA2GIVA*), coding for the arachidonic acid-specific cytosolic phospholipase A2 (cPLA2), was more than 80-fold higher expressed in basal-like xenografts. cPLA2-mediated degradation of PtdCho is a plausible mechanism for the high GPC and GPE concentrations in this model.

DISCUSSION

In this study we implemented in vivo 3D ^{31}P MRSI at 11.7T to investigate the levels of individual phospholipids in patient-derived breast cancer xenografts at sufficient resolution to encompass predominantly tumor tissue. We found a good agreement between in vivo MRSI and in vitro NMR data, which validates that ^{31}P MRSI is suitable for detailed studies of phospholipid metabolism in cancer xenografts. The metabolite differences were associated with differences in expression of the genes involved in PtdCho and PtdEtn metabolism. Luminal-like and basal-like xenografts could be completely separated by this method based on the levels of cholines and ethanolamines.

In ^{31}P MR spectra of xenografts tumors without localization or at low field, it is difficult to separate individual phospholipid metabolites (20). With single voxel localization by the ISIS sequence it may be possible to get a good local field homogeneity so that PCho, PEtn, GPC, and GPE become resolved (14). Performing this technique at higher magnetic fields (13), and with a special experimental setup to prevent air-tissue jumps, that spoil field homogeneity, 1D ^{31}P MRSI with resolved phospholipid peaks can be obtained (12). Here we demonstrated that at a field strength of 11.7T it is possible to perform 3D ^{31}P MRSI of xenografts growing in the mammary fat pad with spectra showing well-resolved signals for the phospholipids PCho, PEtn, GPC, and GPE with good SNR and low PCr, indicating minimal muscle contamination. Although the nominal resolution seems to allow the assessment of spatial tumor heterogeneity, the filtered *k*-space acquisition makes the actual voxel size similar to the tumor size, but the 3D MRSI acquisition does allow an optimal postacquisition voxel place selection. The recent availability of high-field clinical MR scanners, improved gradients, and multichannel radiofrequency coils makes the acquisition of in vivo ^{31}P MRSI from human tumors, including breast tumors, feasible (26–28).

Similar phospholipid metabolic profiles were observed for the in vitro and in vivo-acquired ^{31}P MR spectra, but only in the luminal-like xenograft MR spectra the PEtn and GPC levels showed a significant difference. This might be because the in vitro and in vivo MR experiments were not performed on identical animals. It is unlikely that the extraction process caused these metabolic changes, as the basal-like MR spectra showed similar in vivo and in vitro metabolic profiles. Moreover, the score plot from the PCA clearly shows that the variation in metabolic profile between the in vivo and in vitro measurements is much smaller than the variation between the two xenograft models. The similarity in the spectral features obtained in vivo and in vitro indicates that the phospholipids seen by ^{31}P MRSI are a proper representation of their content in the two breast cancer subtypes. It has been shown that the subtype-specific metabolic profiles observed in xenograft tumors also are present in human breast tumors, emphasizing the potential translational value of ^{31}P MRSI in this field (16).

As cancer biomarkers, phospholipid metabolites are associated with malignancy, survival, and clinical response to neoadjuvant treatment (3,29–31). The abnormal phospholipid metabolism in breast cancer is not understood in detail. Previous studies have focused on PCho and GPC, which are intermediate metabolites in synthesis and degradation of PtdCho. These metabolites are often present in high concentration in cancers, which traditionally has been associated with a high plasma membrane turnover. The abnormal PCho and GPC levels in cancer have been linked to altered enzyme activity, in particular of choline kinase and several phospholipases (3,11). In mammals, ChoK is encoded by two separate genes: *ChoKA* and *ChoKB*, catalyzing the phosphorylation of Cho to PCho (32). The activity of these enzymes depends on oncogenic signaling and microenvironmental parameters such as hypoxia (33). Metabolic

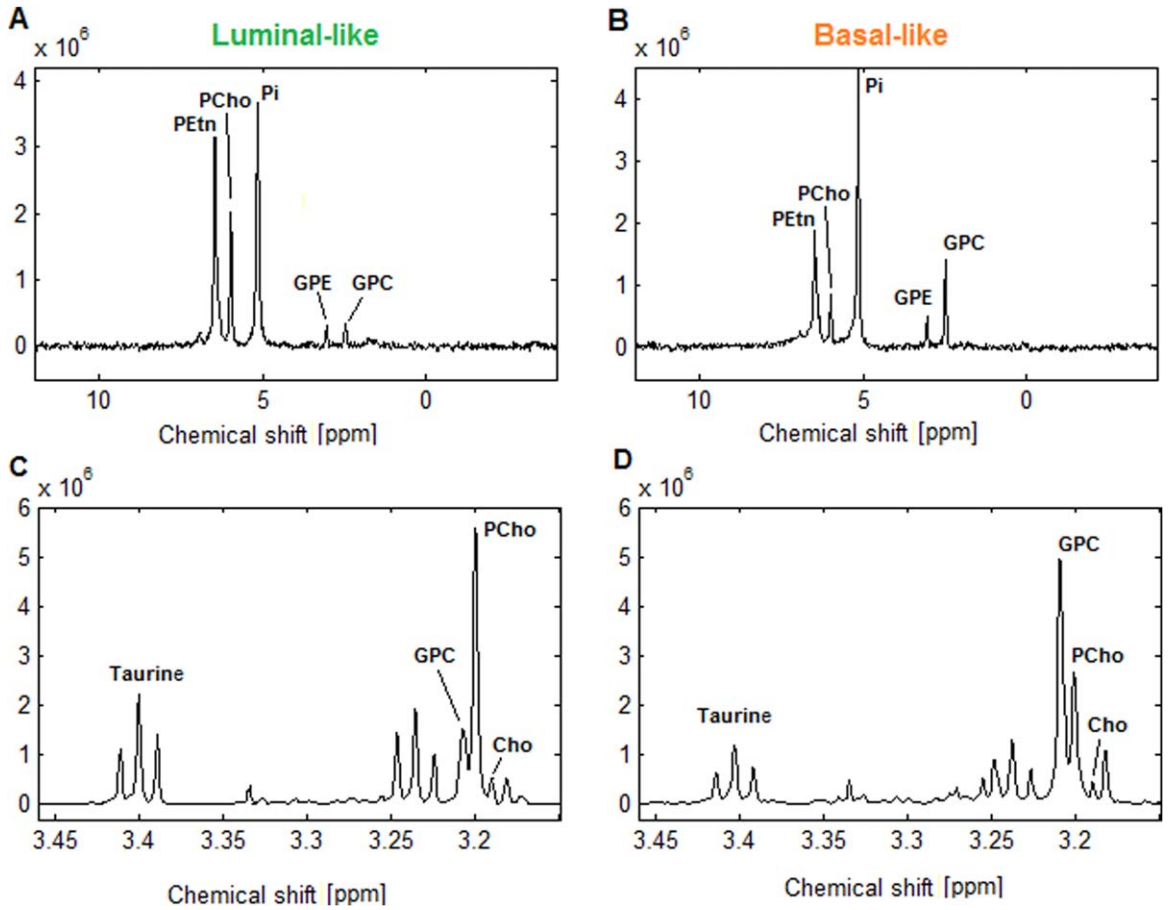

Figure 3. In vitro data obtained from tumor tissue extracts. Examples of ^{31}P NMR spectra of extracts obtained from luminal-like (**A**) and basal-like (**B**) showing the same spectral features observed in vivo. The luminal-like xenografts showed higher PCho and PEtn than GPC and GPE levels as compared with the basal-like xenografts. The inverse relationship between PCho and GPC levels was observed both in ^{31}P NMR and ^{1}H NMR spectra (**C,D**). [Color figure can be viewed in the online issue, which is available at wileyonlinelibrary.com.]

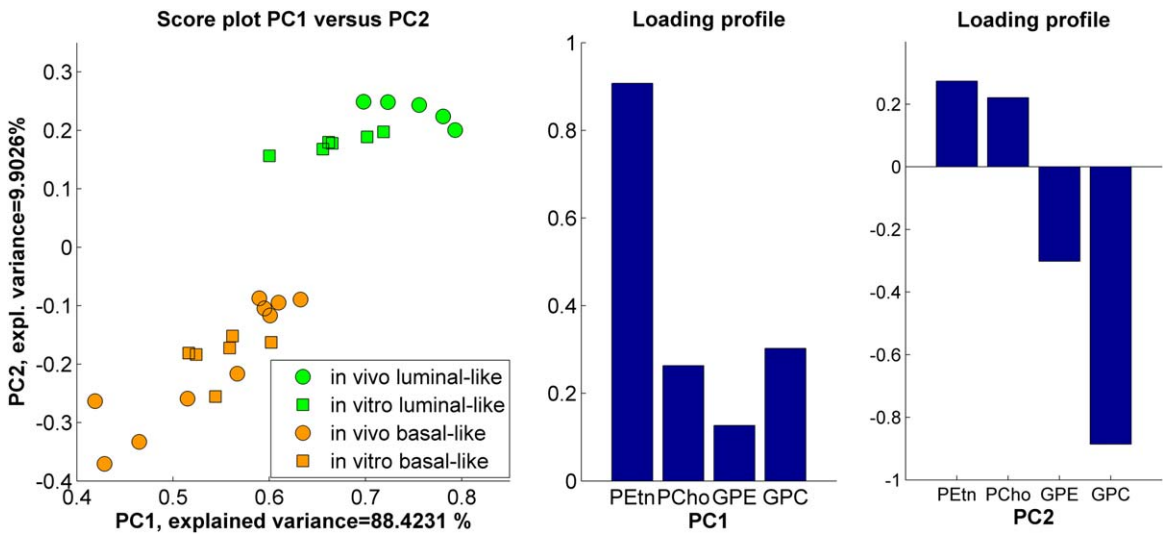

Figure 4. Principle component analysis. **A:** Score plot of the relative metabolite concentrations obtained from ^{31}P MR spectra of xenografts. PCA score plot of the phospholipid metabolites (ie, PEtn, PCho, GPE, and GPC) from both in vivo and in vitro ^{31}P MR spectra clearly discriminates the luminal-like from basal-like xenografts. The variances captured by the PC1 and PC2 were 88.4% and 9.9%, respectively. The clustering of samples from luminal-like (green color) and basal-like (orange color) confirm the relatively similar profile of the phospholipid metabolites in the in vivo and the corresponding in vitro spectra. **B:** Loading profiles of the first and (**C**) second principle components. The corresponding loading profiles of PC1 and PC2 indicate that luminal-like are associated with higher levels of PEtn and lower GPC than the basal-like xenografts. [Color figure can be viewed in the online issue, which is available at wileyonlinelibrary.com.]

Table 1
Differential Expression of Genes Involved in PME and PDE Metabolism

Entrez ID	Gene name	Encoded protein	Log2-fold difference	Adjusted *P*-value
5321	PLA2GIVA	Phospholipase A2, group IV A	6.4	$4.4E^{-16}$
8681	PLA2GIVB	Phospholipase A2, group IV B	0.9	$9.8E^{-5}$
10434	LYPLA1	Lysophospholipase 1	0.9	0.001
151056	PLB1	Phospholipase B1	0.7	0.0001
5337	PLD1	Phospholipase D1	0.7	0.0005
1119	ChoKA	Choline kinase, alpha	−0.3	0.047
11313	LYPLA2	Lysophospholipase II	−0.4	0.005
1119	ChoKB	Choline kinase beta	−0.8	$2.0E^{-6}$
8399	PLA2G10	Phospholipase A2, group X	−1.1	$3.1E^{-6}$
5338	PLD2	Phospholipase D2	−1.1	$1.2E^{-6}$
81579	PLA2G12A	Phospholipase A2, group XII A	−1.6	$2.5E^{-9}$
3647	ETNK1	Ethanolamine kinase 1	−1.7	$6.6E^{-9}$
50487	PLA2GIII	Phospholipase A2, group III	−3.1	$1.1E^{-12}$
14494	ETNK2	Ethanolamine kinase 2	−4.4	$1.6E^{-11}$

Positive log2-fold difference indicates higher expression in basal-like xenografts, while negative log2-fold difference indicates higher expression in luminal-like xenografts.

pathways therefore represent a target for anticancer drugs as exemplified by the preclinical efficacy of drugs targeting choline kinase and cytosolic phospholipase A2 (34,35). PCho and PEtn are precursors of the cell membrane phospholipids phosphatidylcholine (PtdCho) and phosphatidylethanolamine (PtdEtn), but are also formed by degradation of PtdCho and PtdEtn by phospholipase C (PLC) (11). The metabolites PEtn and GPE have also been linked to cancer (11). However, the understanding of PtdEtn metabolism in cancer is still limited, partly because of technical difficulties to detect ethanolamine-containing metabolites by 1D ^{1}H MRS. The spectral resolution of in vivo ^{1}H MRS is not sufficient to separate the overlapping signals of free choline, PCho, and GPC (36). Furthermore, the peaks of PEtn and GPE are not prominent in 1D ^{1}H MRS. The present study demonstrates the ability of ^{31}P MRSI to detect individual phospholipid metabolites in vivo, allowing for a more comprehensive characterization of this metabolic network than ^{1}H MRS. In addition, ^{31}P MRSI may be a useful tool for in vivo therapy monitoring for drugs that directly interfere with choline or ethanolamine metabolism, such as the choline kinase inhibitor MN58b (34).

Metabolic profiling using ^{31}P MRSI can therefore potentially contribute to improved clinical risk stratifications in breast cancer, which in turn can be beneficial in development of personalized treatment strategies (1). Using gene expression analysis, several distinct breast cancer subtypes have previously been identified, including the luminal-like A and B, basal-like and HER2-positive, and a normal-like subtype (37,38). The driving genetic abnormalities vary between breast cancer subtypes (38), which may be reflected in the metabolic profiles and their response to therapy. However, gene expression subtyping has not yet been implemented in clinical practice, as this method alone does not allow identification of patients with particularly good or poor prognosis. A possible future development in this field is algorithms for combining metabolic profiles with other –omics data for subclassification of patients within the currently established subtypes (39).

In this study the expression of genes involved in PtdCho and PtdEtn turnover correlated with the metabolic profiles observed in ^{31}P MR spectra. The inverse PCho-GPC ratio observed in both the in vitro ^{1}H/^{31}P NMR spectra and the in vivo ^{31}P MR spectra agrees with previous studies of these xenografts (16), demonstrating that in vivo ^{31}P MRSI can discriminate between these two breast cancer models. However, the increased GPC level in basal-like xenografts, the aggressive model, is not in accordance with previous ^{1}H/^{31}P MRS studies, which found higher PC/GPC ratios or dominant PME in the triple negative breast cancer cell line MDA-MB-231 (34,40). In our study, the high PCho concentration in luminal-like xenografts was associated with high expression of both *ChoKA* and *ChoKB* (Table 1). Conversion of ethanolamine to PEtn is carried out by *ChoKA/B*, but also *ETNK1/2* (41). All these genes were significantly higher expressed in the luminal-like xenografts, which is consistent with the high PEtn signal found in the MR spectra both in vivo and in vitro.

GPC and GPE are degradation products of PtdCho and PtdEtn, respectively, and have therefore been suggested as indicative markers for the rate of cell membrane turnover. Degradation of PtdCho and PtdEtn by *PLA2GIVA/B, LYPLA1/2*, *PLB1*, *PLA2G3*, *PLA2G10*, and *PLA2G12A* lead to formation of GPC and GPE, respectively. In particular, PLA2GIVA has been associated with cancer, as upregulation of this gene is associated with PI3K signaling, inflammation, and angiogenesis (42). The difference in GPC and GPE concentrations could not be directly elucidated from the gene expression data, as the differential expression of various phospholipases was complex and difficult to interpret. However, the *phospholipase A2 group IVA* (*PLA2GIVA*), coding for the arachidonic acid-specific cytosolic phospholipase A2 (cPLA2), was more than 80-fold higher expressed in basal-like xenografts. cPLA2-mediated degradation of PtdCho is a plausible mechanism for the high GPC and GPE concentrations in this model. *PLA2GIVB, LYPLA1,* and *PLB1* were also higher expressed in the basal-like compared with the luminal-like xenografts (Table 1),

which may explain the high concentrations of GPC and GPE in this model. However, the significant lower expressions of other genes involved in PtdCho degradation; *LYPLA2*, *PLA2G3*, *PLA2G10*, and *PLA2G12A* in basal-like xenografts (Table 1) did not allow a full explanation for higher GPC and GPE levels in this model.

Although ^{31}P MRS enabled in vivo metabolic profiling of two different breast cancer xenografts, its diagnostic specificity remains to be investigated by including more diverse breast cancer models. To assess tumor heterogeneity, further improvement of the spatial resolution is needed, which may be possible by still better coil designs and use of ^{1}H-^{31}P polarization transfer (43) or nuclear Overhauser enhancement (44).

In conclusion, we demonstrated that localized in vivo 3D ^{31}P MRSI at 11.7T could be used to discriminate between basal-like and luminal-like breast cancer xenografts. The in vivo metabolic profiles, reflecting the concentration of PCho, PEtn, GPC, and GPE, were in agreement with in vitro NMR results obtained from the same xenograft models. In addition, gene expression analysis showed a correlation between the expression levels of some genes and the observed metabolic profiles. Metabolic profiling using ^{31}P MRS can be a tool for improved subtyping and, perhaps in the future, therapeutic monitoring in cancer.

ACKNOWLEDGMENTS

The authors thank Jeroen Mooren and Bianca Lemmers van de Weem for biotechnical assistance during the animal experiments. The authors thank Sjaak van Asten for technical assistance with MR measurements, Lars Evje for help with tissue extractions, and Dr. Therese Sørlie for gene expression analysis. The in vitro analyses were performed at the MR Core Facility, Norwegian University of Science and Technology (NTNU). The in vivo work was performed in the Preclinical Imaging Centre (PRIME), St. Radboud University Nijmegen as part of the EuroBioImaging Proof of Concept program.

REFERENCES

1. Bathen TF, Sitter B, Sjobakk TE, Tessem MB, Gribbestad IS. Magnetic resonance metabolomics of intact tissue: a biotechnological tool in cancer diagnostics and treatment evaluation. Cancer Res 2010;70:6692–6696.
2. Beloueche-Babari M, Chung YL, Al-Saffar NM, Falck-Miniotis M, Leach MO. Metabolic assessment of the action of targeted cancer therapeutics using magnetic resonance spectroscopy. Br J Cancer 2010;102:1–7.
3. Glunde K, Bhujwalla ZM, Ronen SM. Choline metabolism in malignant transformation. Nat Rev Cancer 2011;11:835–848.
4. Herminghaus S, Pilatus U, Moller-Hartmann W, et al. Increased choline levels coincide with enhanced proliferative activity of human neuroepithelial brain tumors. NMR Biomed 2002;15:385–392.
5. McKnight TR, Smith KJ, Chu PW, et al. Choline metabolism, proliferation, and angiogenesis in nonenhancing grades 2 and 3 astrocytoma. J Magn Reson Imaging 2011;33:808–816.
6. Heerschap A, Jager GJ, van der Graaf M, et al. In vivo proton MR spectroscopy reveals altered metabolite content in malignant prostate tissue. Anticancer Res 1997;17:1455–1460.
7. Kurhanewicz J, Swanson MG, Nelson SJ, Vigneron DB. Combined magnetic resonance imaging and spectroscopic imaging approach to molecular imaging of prostate cancer. J Magn Reson Imaging 2002;16:451–463.
8. Kvistad KA, Bakken IJ, Gribbestad IS, et al. Characterization of neoplastic and normal human breast tissues with in vivo (1)H MR spectroscopy. J Magn Reson Imaging 1999;10:159–164.
9. Baek HM, Chen JH, Nie K, et al. Predicting pathologic response to neoadjuvant chemotherapy in breast cancer by using MR imaging and quantitative 1H MR spectroscopy. Radiology 2009;251:653–662.
10. Esmaeili M, Bathen TF, Engebraten O, Maelandsmo GM, Gribbestad IS, Moestue SA. Quantitative 31 P HR-MAS MR spectroscopy for detection of response to PI3K/mTOR inhibition in breast cancer xenografts. Magn Reson Med 2013 [Epub ahead of print].
11. Podo F. Tumour phospholipid metabolism. NMR Biomed 1999; 12:413–439.
12. Silberhumer GR, Zakian K, Malhotra S, et al. Relationship between 31P metabolites and oncolytic viral therapy sensitivity in human colorectal cancer xenografts. Br J Surg 2009;96:809–816.
13. Lee SC, Huang MQ, Nelson DS, et al. In vivo MRS markers of response to CHOP chemotherapy in the WSU-DLCL2 human diffuse large B-cell lymphoma xenograft. NMR Biomed 2008;21: 723–733.
14. Morse DL, Carroll D, Day S, et al. Characterization of breast cancers and therapy response by MRS and quantitative gene expression profiling in the choline pathway. NMR Biomed 2009;22: 114–127.
15. Sorlie T. Molecular portraits of breast cancer: tumour subtypes as distinct disease entities. Eur J Cancer 2004;40:2667–2675.
16. Moestue SA, Borgan E, Huuse EM, et al. Distinct choline metabolic profiles are associated with differences in gene expression for basal-like and luminal-like breast cancer xenograft models. BMC Cancer 2010;10:433.
17. Bergamaschi A, Hjortland GO, Triulzi T, et al. Molecular profiling and characterization of luminal-like and basal-like in vivo breast cancer xenograft models. Mol Oncol 2009;3:469–482.
18. Staewen RS, Johnson AJ, Ross BD, Parrish T, Merkle H, Garwood M. 3-D FLASH imaging using a single surface coil and a new adiabatic pulse, BIR-4. Invest Radiol 1990;25:559–567.
19. Gruetter R. Automatic, localized in vivo adjustment of all first- and second-order shim coils. Magn Reson Med 1993;29:804–811.
20. Boer VO, van de Bank BL, van Vliet G, Luijten PR, Klomp DW. Direct B0 field monitoring and real-time B0 field updating in the human breast at 7 Tesla. Magn Reson Med 2012;67:586–591.
21. Naressi A, Couturier C, Devos JM, et al. Java-based graphical user interface for the MRUI quantitation package. MAGMA 2001; 12:141–152.
22. Vanhamme L, van den Boogaart A, Van Huffel S. Improved method for accurate and efficient quantification of MRS data with use of prior knowledge. J Magn Reson 1997;129:35–43.
23. Gribbestad IS, Petersen SB, Fjosne HE, Kvinnsland S, Krane J. 1H NMR spectroscopic characterization of perchloric acid extracts from breast carcinomas and non-involved breast tissue. NMR Biomed 1994;7:181–194.
24. Marshall I, Higinbotham J, Bruce S, Freise A. Use of Voigt lineshape for quantification of in vivo 1H spectra. Magn Reson Med 1997;37:651–657.
25. Kanehisa M, Goto S. KEGG: kyoto encyclopedia of genes and genomes. Nucleic Acids Res 2000;28:27–30.
26. Klomp DW, van de Bank BL, Raaijmakers A, et al. 31P MRSI and 1H MRS at 7 T: initial results in human breast cancer. NMR Biomed 2011;24:1337–1342.
27. Wijnen JP, van der Kemp WJ, Luttje MP, Korteweg MA, Luijten PR, Klomp DW. Quantitative 31P magnetic resonance spectroscopy of the human breast at 7 T. Magn Reson Med 2012;68:339–348.
28. Kobus T, Bitz AK, van Uden MJ, et al. In vivo 31P MR spectroscopic imaging of the human prostate at 7 T: safety and feasibility. Magn Reson Med 2012;68:1683–1695.
29. Kumar M, Jagannathan NR, Seenu V, Dwivedi SN, Julka PK, Rath GK. Monitoring the therapeutic response of locally advanced

breast cancer patients: sequential in vivo proton MR spectroscopy study. J Magn Reson Imaging 2006;24:325–332.
30. Tozaki M, Sakamoto M, Oyama Y, Maruyama K, Fukuma E. Predicting pathological response to neoadjuvant chemotherapy in breast cancer with quantitative 1H MR spectroscopy using the external standard method. J Magn Reson Imaging 2010;31: 895–902.
31. Wijnen JP, Idema AJ, Stawicki M, et al. Quantitative short echo time 1H MRSI of the peripheral edematous region of human brain tumors in the differentiation between glioblastoma, metastasis, and meningioma. J Magn Reson Imaging 2012;36:1072–1082.
32. Aoyama C, Liao H, Ishidate K. Structure and function of choline kinase isoforms in mammalian cells. Prog Lipid Res 2004;43: 266–281.
33. Jiang L, Greenwood TR, Artemov D, et al. Localized hypoxia results in spatially heterogeneous metabolic signatures in breast tumor models. Neoplasia 2012;14:732–741.
34. Al-Saffar NM, Troy H, Ramirez de Molina A, et al. Noninvasive magnetic resonance spectroscopic pharmacodynamic markers of the choline kinase inhibitor MN58b in human carcinoma models. Cancer Res 2006;66:427–434.
35. Patel MI, Singh J, Niknami M, et al. Cytosolic phospholipase A2-alpha: a potential therapeutic target for prostate cancer. Clin Cancer Res 2008;14:8070–8079.
36. Begley JK, Redpath TW, Bolan PJ, Gilbert FJ. In vivo proton magnetic resonance spectroscopy of breast cancer: a review of the literature. Breast Cancer Res 2012;14:207.
37. Perou CM, Sorlie T, Eisen MB, et al. Molecular portraits of human breast tumours. Nature 2000;406:747–752.
38. Sorlie T, Tibshirani R, Parker J, et al. Repeated observation of breast tumor subtypes in independent gene expression data sets. Proc Natl Acad Sci U S A 2003;100:8418–8423.
39. Borgan E, Sitter B, Lingjaerde OC, et al. Merging transcriptomics and metabolomics—advances in breast cancer profiling. BMC Cancer 2010;10:628.
40. Glunde K, Jie C, Bhujwalla ZM. Molecular causes of the aberrant choline phospholipid metabolism in breast cancer. Cancer Res 2004;64:4270–4276.
41. Aoyama C, Nakashima K, Ishidate K. Molecular cloning of mouse choline kinase and choline/ethanolamine kinase: their sequence comparison to the respective rat homologs. Biochim Biophys Acta 1998;1393:179–185.
42. Linkous A, Yazlovitskaya E. Cytosolic phospholipase A2 as a mediator of disease pathogenesis. Cell Microbiol 2010;12: 1369–1377.
43. Wijnen JP, Scheenen TW, Klomp DW, Heerschap A. 31P magnetic resonance spectroscopic imaging with polarisation transfer of phosphomono- and diesters at 3 T in the human brain: relation with age and spatial differences. NMR Biomed 2010;23:968–976.
44. Hattingen E, Lanfermann H, Menon S, et al. Combined 1H and 31P MR spectroscopic imaging: impaired energy metabolism in severe carotid stenosis and changes upon treatment. Magma 2009;22:43–52.